Catalysis Today 426 (2024) 114366

Contents lists available at ScienceDirect

Catalysis Today

journal homepage: www.elsevier.com/locate/cattod

Sulphur poisoning and regeneration of Li-Ru/Al_2O_3 dual function material for the integrated CO_2 capture and methanation

Stefano Cimino *, Elisabetta Maria Cepollaro, Milena Pazzi, Luciana Lisi

CNR-STEMS Science and Technology for Sustainable Energy and Mobility, Via G. Marconi 4, 80125 Napoli, Italy

ARTICLE INFO

Keywords:
CO_2 Capture and Utilization
Renewable Methane
Chemical Looping
Ruthenium
Sulfur Poisoning
Catalyst Regeneration

ABSTRACT

Effective integration of the CO_2 capture from flue gases and its subsequent methanation with renewable H_2 to achieve a net-zero chemical looping process poses strong challenges in the development of highly performing Dual Function Materials (DFMs). Li-Ru/Al_2O_3 DFM has been shown to optimally operate the cyclic process at low temperature (260 – 280 °C) with stable performance upon ageing and outstanding tolerance to SO_x impurities in the flue gas, which, however, slowly deteriorate its CO_2 capture capacity. This work investigates the mechanisms behind the sulfur-poisoning and self-regeneration capability of the catalytic features of the Li-Ru DFM as well as the irreversible inhibition of CO_2 adsorption. Eventually, we demonstrate the remarkable effectiveness of a simple ex-situ regeneration procedure for a heavily sulfur-aged DFM aiming to minimize the consumption of critical raw materials within a circular economy approach.

1. Introduction

CO_2 Capture and Utilization (CCU) is included in the leading technologies required for a transition to climate neutrality because it potentially enables a net CO_2 consumption and, at the same time, virtuous recycling [1]. The challenge is to convert CO_2 from industrial processes or air into synthetic fuels using renewable energy-driven processes approaching a circular carbon economy [1–4]. This is also an efficient solution to chemically store excess renewable energy that is generally fluctuating and seasonal. However, current CCU technologies using conventional multistage processes are highly energy intensive (particularly for sorbent regeneration and CO_2 purification/compression), and their associated costs are still considerable [3–5]. Recently, the integration of CO_2 capture and its in-situ conversion into a single chemical looping process producing methane or other valuable fuels has been proposed as an innovative solution to cut energy costs and increase the efficiency of CCU [3–10]. Dual Function Materials (DFMs) are required to operate the looping process, which can alternatively capture CO_2 from dilute streams and then catalytically hydrogenate it at the same temperature when exposed to H_2 [11,12]. In particular, it has been demonstrated that the integrated CO_2 capture and methanation (ICCM) can be performed at moderate temperatures (250 – 400 °C) over DFMs which contain a catalytic metal (e.g. Ni or Ru) and a CO_2 sorbent phase (e.g. alkali (hydro)oxides/carbonates) closely coupled and finely dispersed on alumina support [8–21]. Since both the CO_2 adsorption and its methanation are exothermic, the ICCM process can be run by harvesting the sensible heat of typical flue gases without any external energy input (apart from that needed to produce renewable H_2) [8–15]. Parallel fixed bed reactors with alternate feeds [8,9,11–13] or interconnected fluidized bed reactors with circulating DFMs [10,14] can be used to operate the ICCM continuously.

To design highly performing DFMs it is vital to investigate realistic operating conditions to anticipate stability issues and deactivation modes [8,16,20–24]. In particular, during the CO_2 capture stage from a point source or even from the air, the DFM is exposed to O_2 and water vapour at concentrations and temperatures that vary with the specific application [16]. Supported Ni catalysts suffer irreversible oxidation (and deactivation) during CO_2 capture in the presence of O_2 at the typical temperatures of ICCM [20]. Therefore, Ru is generally preferred to Ni despite its higher cost, since its oxide can be easily reduced back to the active metallic form during the methanation step already at ca 150 °C [16,18–20]. However, the low availability of Ru inevitably limits its maximum loading in the DFM, and some sintering issues have been recently reported upon long-term hydrothermal ageing under cyclic operation at 320 °C [22]. Moreover, in several practical scenarios, impurities such as SO_x and NO_x may be present at ppm levels even after purification units, and they must be carefully considered since they can drastically impact process performance, design and economics [16,24,

* Corresponding author.
E-mail address: stefano.cimino@cnr.it (S. Cimino).

https://doi.org/10.1016/j.cattod.2023.114366
Received 21 April 2023; Received in revised form 14 July 2023; Accepted 1 September 2023
Available online 4 September 2023

26–29]. Recent studies have demonstrated that NO_x just compete with CO_2 for the same adsorption sites, which are finally regenerated upon H_2 exposure [27,28]. At variance, SO_x can impact both the sorption and the catalytic functions of the DFM: in particular, the selective S-poisoning of Ru-, Rh- and Ni- supported catalysts under reducing atmospheres is well-known and due to the formation of surface metal sulfide phases, which are inactive for steady-state reforming and methanation [24, 29–33]. For this last reaction, Ru can be (partly) regenerated by a periodic oxidative treatment at mild conditions (ca 300 °C) that decompose RuS_x directly into RuO_x and SO_2 without forming stable metal sulfides [32,33] at variance to Ni [29,31]. The support can also play an important role by possibly acting as S-scavenger, thus protecting to some extent the Ru active sites from poisoning as in the case of Al_2O_3 but not SiO_2 [33]. Interestingly, the accumulation of sulfates on the support exposes the catalyst to the risk of a self-poisoning effect even under S-free methanation conditions [32].

We have recently reported for the first time that Ru/Al_2O_3 DFMs containing either Na or Li as the CO_2 sorbent phase display a remarkable sulfur tolerance during cyclic operation of the ICCM with a flue gas containing SO_2 (up to 100 ppmv) in combination with O_2 and H_2O [24, 34]. In particular, SO_2 is captured and stored on the DFM preventing any significant poisoning effect during the methanation phase at 280 – 300 °C. The Li-based DFM outperforms its Na-counterpart at fixed alkali and Ru contents since it can be operated at lower temperatures showing higher CO_2 capture capacity, methane productivity and sulfur tolerance [34]. However, the saturation of the strong basic sites by sulfates irreversibly deteriorates the CO_2 capture capacity of the DFM in the long term [24,34]. The low availability and high price of critical raw materials such as Ru (and Li) require to reuse or recycle them within a sustainable circular economy approach. To this end, in this work, we set out to investigate the efficacy of a facile ex-situ regeneration treatment for a heavily sulfated $Li\text{-}Ru/Al_2O_3$ DFM, which consists of washing in water at room temperature to remove soluble Li-sulfate species, followed by re-impregnation with Li-nitrate solution to replenish the original alkali content. Tests of the Integrated CO_2 Capture and Methanation process over the fresh and the regenerated DFM were run in a fixed bed operated at 260 °C with S-free alternate feeds. A detailed characterization of the S-aged, washed and regenerated samples was performed by combining results from ex-situ (ICP-MS, XRD, N_2-physisorption, TG-MS, FT-IR) and operando techniques (transient DRIFT analysis, catalytic methanation tests with co-fed CO_2-H_2) to get insights into the mechanisms behind the resilience of the DFM to sulfur poisoning during the ICCM and the regeneration of both its adsorption and catalytic features.

2. Experimental

2.1. Preparation of the Li-Ru/Al_2O_3 dual function material and its regeneration

Ruthenium (ca 1% wt.) and then Lithium (3% wt.) were sequentially dispersed on the porous matrix of γ-Al_2O_3 spherical particles (Sasol, 1 mm nominal diameter) as already described in [34] by an incipient wetness impregnation method using water solutions of the corresponding nitrate precursors followed by calcination in air at 350 °C and a final reduction at 450 °C under a flow of 20% H_2 in N_2.

The S-aged DFM used for this work was preliminaly subjected to a total of 108 alternated CO_2 capture and methanation cycles in a fixed bed reactor operated at 280 °C with a feed containing O_2, H_2O and up to 100 ppm SO_2, as reported in details elsewhere [34]. A portion of the S-aged DFM recovered from the ICCM reactor at the end of the experimental campaign was washed in deionized water to remove soluble sulfur species (1 g of DFM in 30 cm^3 hold at room temperature overnight, then rinsed with water and finally dried at 120 °C). The concentration of Li, Ru, and sulfate species dissolved in the supernatant solution was analyzed by ICP-MS (Agilent 7000) and Ionic Chromatography (Metrhom 883 Basic IC Plus), respectively.

Ultimately, after washing, the regeneration of the DFM was completed by restoring its initial lithium content via a novel incipient wetness impregnation step with an appropriate Li-nitrate water solution, followed by drying at 120 °C, and reduction at 450 °C for 2 h under a 20% H_2 in N_2 flow.

2.2. Characterization of the DFMs

The true density of DFM spheres (Fresh, S-aged, Washed, Regenerated) was estimated by weighing a known number (ca 100) of spheres with a nominally identical volume after stabilization in ambient air for more than 24 h.

N_2 adsorption-desorption measurements at − 196 °C were performed in a Quantachrome Autosorb 1-C after degassing the DFM samples at 150 °C for 3 h under a high dynamic vacuum. The specific surface area and pore size distribution (PSD) of the DFMs were evaluated by the BET method and the Non-Linear Density Function Theory (NLDFT, cylindrical pore, equilibrium model), respectively.

X-ray diffraction (XRD) measurements were performed on powdered DFM samples using a Rigaku Miniflex 600 diffractometer with Cu Kα radiation (0.154 nm wavelength). XRD patterns were collected in a 2θ range of 10 – 80°, with a step of 0.01° and 10° min^{-1} counting time. Background correction, fitting, and peak attribution were performed using SmartLab Studio II software. The average crystallite sizes of Ru and (Li)Al_2O_3 phases were estimated based on Scherrer's equation from the full width at half maximum (FWHM) of their corresponding main reflections occurring at $2\theta = 43.9°$ [1 0 1] and $2\theta = 66.9°$ [4 4 0], respectively.

A flow microbalance (Setaram Labsys Evo TGA-DTA-DSC 1600) was used to perform temperature-programmed reaction tests with DFM samples (90–100 mg) under a flow of 4.5% H_2/Ar (50 cm^3 min^{-1}) up to 750 °C at a rate of 10 °C min^{-1}. The evolved gases were continuously analyzed by a Mass Spectrometer (Pfeiffer Thermostar G) equipped with a Secondary Electron Detector (MS-SEM).

FT-IR analysis was performed on self-supported disks of KBr mixed with 2% wt. of powdered DFM samples (stabilized in air at room temperature) using a Perkin Elmer Spectrum 3 instrument equipped with a DTGS detector. Each spectrum (resolution of 4 cm^{-1}) was averaged over 64 scans and ratioed against the common background relevant to pure KBr.

Operando DRIFT analysis during the cyclic CO_2 capture and methanation process was performed at 300 °C on fresh and S-aged DFMs that were loaded (as powders, ca 50 mg) in a heated reaction chamber equipped with a ZnSe window (PiKe DRIFT). IR spectra were acquired with a Perkin Elmer Spectrum GX instrument using a N_2-cooled MCT detector (4 cm^{-1} resolution, averaging over 64 scans). Preliminarily, each DFM sample was reduced at 400 °C under a flow of 2% H_2/N_2, then purged with Ar and cooled to the reaction temperature (300 °C) where a background spectrum was acquired after stabilizing for 30 min (under Ar flow). Thereafter, the reaction sequence included a carbonation step for 60 min under 15% CO_2/N_2 flow, followed by purging for 30 min with Ar, and a final hydrogenation step for 60 min under 2% H_2/N_2 flow.

2.3. Cycled CO_2 capture and methanation tests in the fixed bed reactor

Integrated CO_2 capture and methanation tests were performed at atmospheric pressure in a fixed bed reactor that was packed with a fixed volume of DFM spheres (0.6 cm^3) to keep constant the Ru loading regardless of the density of the specific DFM sample. The reactor was operated isothermally at 260 °C with alternate feed conditions at a constant total flow rate (20 Sdm^3 h^{-1}) [34]. Briefly, a feed gas stream containing 5% vol. CO_2 and 0.25% O_2 in N_2 was stepwise admitted to the reactor and flowed over the DFM for 18 min, followed by 2 min of purging under pure N_2. Thereafter, the feed was switched to 15% vol. H_2 in N_2 for a total of 14 min to convert the CO_2 previously captured on the DFM into methane while regenerating the CO_2 adsorption sites for the

next cycle.

The molar fractions of CO_2, CH_4, CO were continuously measured using an ABB Optima Advance gas analyzer equipped with ND-IR detectors. The amounts of CO_2 captured by the DFM and those of CH_4 and CO formed during the hydrogenation phase were calculated by integrating the temporal concentration traces after correction for the gas hold-up in the empty reactor. The overall carbon balance was generally closed within ± 2%. The CO_2 conversion and the selectivity to CH_4 were calculated based on the total carbon species released according to the formulas:

$$CO_2 \text{ conversion } \% = 100 \cdot (n_{CH4}+n_{CO})/(n_{CH4}+n_{CO}+n_{CO2\ des})$$

$$CH_4 \text{ selectivity } \% = 100 \cdot n_{CH4}/(n_{CH4}+n_{CO})$$

where n_{CH4} and n_{CO} represent the moles of CH_4 and CO formed, and $n_{CO2\ des}$ corresponds to the moles of (unconverted) CO_2 desorbed from the DFM in the product gas during the hydrogenation step.

2.4. Catalytic CO_2 methanation tests

Temperature-programmed methanation tests of gaseous CO_2 + H_2 mixtures were run in the same fixed bed quartz reactor packed with 0.6 cm^3 of DFM spheres. Reaction tests were performed at ca 3 °C min^{-1} from 200 °C to 400 °C under a flow of $CO_2/H_2/N_2 = 1/4/5$ that was fed to the reactor at a Gas Hourly Space Velocity (GHSV) = 33000 h^{-1}. Repeated tests were run over the S-aged DFM sample in the following sequence: #1 without any pre-treatment; #2 and #4 after being exposed to reaction conditions at 400 °C for 30 min (labelled as _Rd and Rd_2, respectively); #3 after a pre-oxidation treatment in air at 300 °C for 30 min (labelled as_Ox).

Low conversion data (<10%) were used to estimate the rate of the catalytic CO_2 consumption per unit volume of the DFM as a function of the reaction temperature under the assumptions of differential conditions and constant molar flow rate [35]. The apparent activation energy for the catalytic CO_2 hydrogenation was estimated from the slope of the corresponding Arrhenius plot.

3. Results and discussion

3.1. Integrated CO_2 capture and methanation in the fixed bed reactor

The average results of 3 consecutive integrated CO_2 capture and methanation cycles run at 260 °C with samples of the fresh, the S-aged, and the regenerated DFM are summarized in Fig. 1 reporting the amounts of the CO_2 captured, the CH_4 produced and the resulting CO_2 conversion during the hydrogenation stage. In each case, no CO was formed confirming the very high methane selectivity of the Li-Ru DFM at 260 °C even after prolonged ageing in the presence of SO_2 [34].

In particular, the fresh DFM captured ca 295 μmol of CO_2 per cm^3 of packed bed, and produced ca 189 μmol cm^{-3} of CH_4 during the subsequent hydrogenation phase, achieving an outstanding 94% conversion of the CO_2 that was retained after the intermediate purging. As reported in our previous study, the Li-Ru DFM showed a remarkable sulfur tolerance when operating the adsorption stage with a simulated flue gas containing up to 100 ppmv of SO_2 together with O_2 and H_2O [34]. Sulfur species were completely captured and stored on the DFM without any evident adverse effect on the CO_2 conversion and the selectivity to CH_4 during the catalytic hydrogenation stage [34]. However, the accumulation of sulfur progressively reduced the CO_2 capture capacity of the DFM by irreversibly blocking its basic adsorption sites. Specifically, the S-aged DFM sample tested in this work had captured as much as 800 μmol g^{-1} of sulfur during ICCM operation [34]. Accordingly, Fig. 1 shows its CO_2 capture capacity, as well as the CH_4 production, dropped to ca 25% of their corresponding initial values recorded over the fresh DFM, whereas the CO_2 conversion remained above 90% showing only a marginal decay.

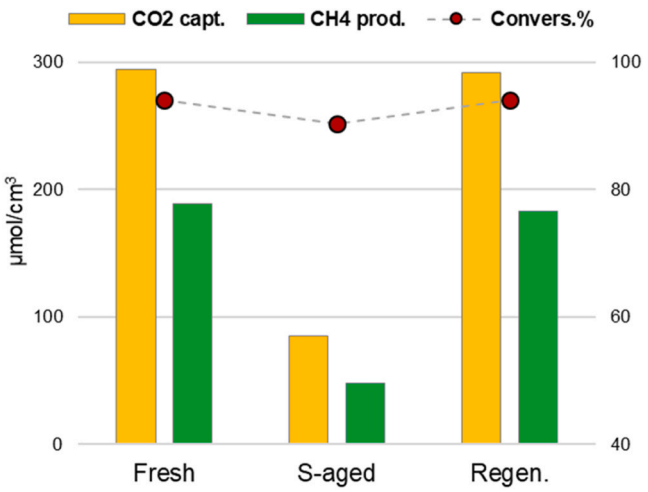

Fig. 1. Average values of CO_2 captured and CH_4 produced as well as CO_2 conversion during 3 consecutive cycles of integrated CO_2 capture and methanation at 260 °C over fresh, S-aged and regenerated Li-Ru DFM. Feed sequence: 5% CO_2 + 0.25% O_2 in N_2 for 18 min (adsorption); pure N_2 for 2 min (purge); 15% H_2 in N_2 for 14 min (hydrogenation).

Eventually, the ex-situ regeneration treatment performed on the S-aged sample allowed to effectively remove the sulfate species and replenish the Li-content up to the original loading in the fresh DFM (see next paragraph). As a result, Fig. 1 shows the regenerated DFM fully recovered the original performance of the fresh sample in terms of CO_2 capture capacity, CH_4 production and CO_2 conversion level during the integrated capture and methanation cycles at as low as 260 °C under S-free feed conditions.

3.2. Characterization of S-aged and regenerated DFMs

The main results of the chemical, morphological and textural characterization of the S-aged, washed and regenerated DFM samples are reported in Table 1 and in Fig. 2 in comparison with the fresh material. Prolonged exposure to SO_2-containing flue gas during the capture stage caused the accumulation of sulfur via reaction with the basic Li-surface sites on the DFM to form crystalline Li_2SO_4 species confirmed by the appearance in the corresponding XRD pattern (Fig. 2a) of the main characteristic signals at 2θ values around 17.5, 21.5, 23.2 and 25° (PDF 15–873). Accordingly, TG analysis of the S-aged DFM under H_2/N_2 flow (Fig. 2b) showed, after an initial dehydration [34], a clear weight loss event (−5.1%) starting from ca 470 °C and completed at 700 °C, which was due to the reactive decomposition of Li_2SO_4 (releasing SO_2, H_2S and H_2O [34]) and corresponded to a S content in the sample of ca 2% (Table 1). The Li-Ru DFM was quite stable during the prolonged ageing under ICCM reaction conditions that induced only minor modifications to the textural features: the original pore size distribution was mostly preserved (Fig. 2c), while the small reduction (−8%) of the specific surface area corresponded to the increase of density of the sample (Table 1) due sulfates accumulating in the mesopores without clogging them. However, XRD analysis suggests that the repeated redox cycling during the ICCM possibly caused a moderate sintering of the Ru nanoparticles in the aged DFM, whose characteristic average dimensions were estimated by the Scherrer's equation to increase from ca 11 up to 15 nm (Table 1).

Given the stability of the sulfate species on the S-aged DFM under both oxidizing and reducing reaction conditions, their removal was attempted ex-situ by a mild washing treatment in deionized water at room temperature, taking advantage of their expected high solubility. Analysis of the concentration of the ionic species in the supernatant solution confirmed the dissolution of Li^+ and SO_4^{2-} species (with a molar ratio of 2.2, slightly above the stoichiometric value in Li_2SO_4).

Table 1
Summary of the characterization results for Fresh, S-aged, Washed, and Regenerated Li-Ru DFM samples: Density of the DFM spheres, Specific surface area (S_{BET}), mesopore volume (V_{mesoP}), and pore width by N_2 physisorption; dimensions of Ru (d_{Ru}) and Al_2O_3 (d_{Al2O3}) crystallites from XRD data; Sulfur content by thermogravimetry; temperatures for 10% conversion (T_{10}) during the catalytic hydrogenation of gaseous CO_2 and corresponding apparent activation energy values (E_a).

Li-Ru DFM	Density g cm^{-3}	S_{BET} m^2 g^{-1}	V_{mesoP} cm^3 g^{-1}	Pore width (mode) nm	d_{Ru} nm	d_{Al2O3} nm	S content % wt.	T_{10} °C	E_a kJ mol^{-1}
Fresh	1.53	145	0.40	10.9	10.6	6.4	-	265	81
S-aged	1.59	133	0.36	11.3	16.5[a]	6.6	2.1[b]	303[c]	68[c]
Washed	1.46	162	0.41	11.3	14.9	6.6	$\leq$ 0.1[b]	299	69
Regenerated	1.53	141	0.41	11.9	15.3	6.8		266	81

[a] possibly over-estimated for an overlapping signal from Li_2SO_4
[b] estimated from TG-MS analysis supposing the decomposition of Li_2SO_4 into Li_2O
[c] S-aged DFM sample recovered to air and tested without any further pretreatment

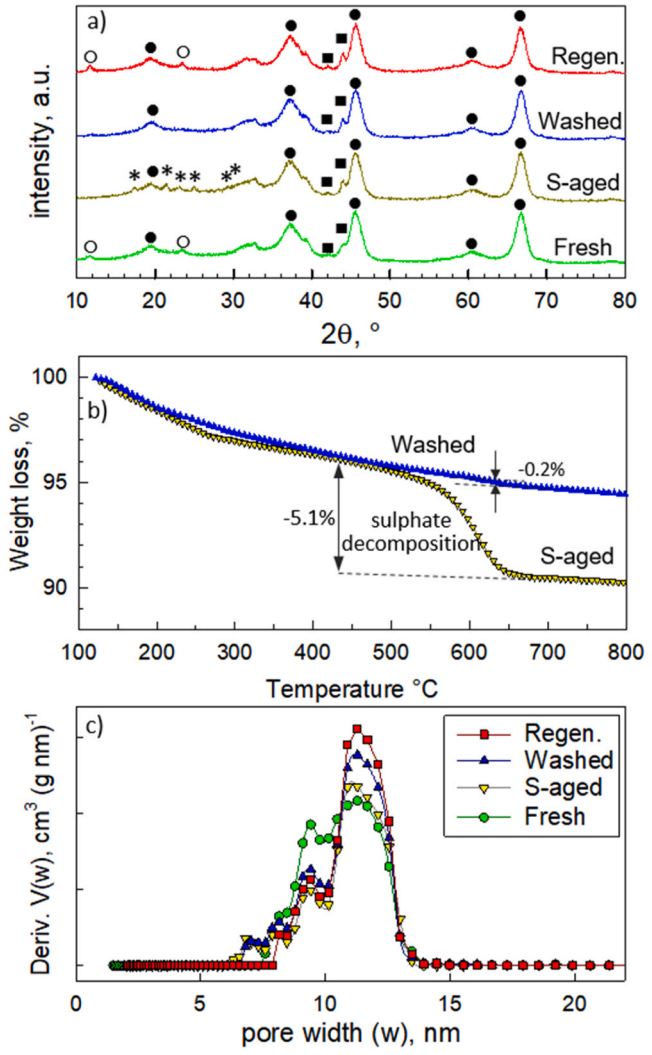

Fig. 2. a) XRD patterns, b) Weight change during the H_2-temperature programmed reduction, and c) Pore Size Distribution analysis of the fresh, S-aged, washed and regenerated Li-Ru DFM samples. XRD legend: ■ =Ru, ○ = γ-Al_2O_3, ⋆ =Li_2SO_4, • = $LiAl_5O_8$. Experimental details can be found in Section 2.2.

Accordingly, TG analysis of the washed DFM sample (Fig. 2b) indicated a residual amount of S below 0.1% wt., corresponding to a S-removal efficiency exceeding 96%. The residual Li-content in the DFM was estimated close to 73% of the original level. Notably, ICP-MS analysis showed that Ru leaching in water was minimal and the DFM retained more than 99.7% of its precious metal content. Therefore, all the signals relevant to Li_2SO_4 disappeared from the XRD pattern of the washed DFM, which closely resembles the fresh sample apart from the absence of two small signals at 11.7 and 23.5°: those features corresponded to the hydrotalcite-like compound $Li_2Al_4(CO_3)(OH)_{12}3\,H_2O$ (Lithium Aluminum Carbonate Hydroxide Hydrate, PDF# 37–728), which spontaneously formed on the fresh DFM upon exposure to ambient air by reaction of surface Lithium aluminate (hydro)oxides with CO_2 and humidity [35]. Interestingly, the regeneration treatment fully restored those reactive Li-species capable to form the Lithium Aluminum Carbonate Hydroxide (red spectrum in Fig. 2a) while also preserving the characteristic average size of Ru crystallites in the DFM (Table 1). Moreover, the regenerated DFM recovered all the original textural features of the fresh DFM (in particular the BET surface area) showing only a small enlargement of the average pore size which was probably due to the reaction of some added Li with residual γ-alumina to form more Li-aluminate spinel phase [35].

The effectiveness of the regeneration procedure was further checked by comparing the FTIR spectra of the S-aged, washed, and regenerated DFM after stabilization in air at room temperature (Fig. 3). The intense spectral feature in the range 1300–1050 cm^{-1} characterizing the spectrum of the S-aged DFM was unambiguously assigned to the formation of Li_2SO_4 [34] and it was coupled to a significant decrease of the carbonate bands in the 1600–1300 cm^{-1} region since the alkali sulfate hinders CO_2 adsorption from the atmosphere [34]. At variance, the bending vibration of absorbed H_2O at 1634 cm^{-1} [36] was substantially unaffected. Some residual sulfates were still present in the washed DFM before rinsing, but they were almost completely absent in the regenerated sample.

As a consequence of the simultaneous removal of both superficial lithium and sulfate species, the spectral region of the adsorbed carbonates on the washed DFM was rather flat and closely resembled that of

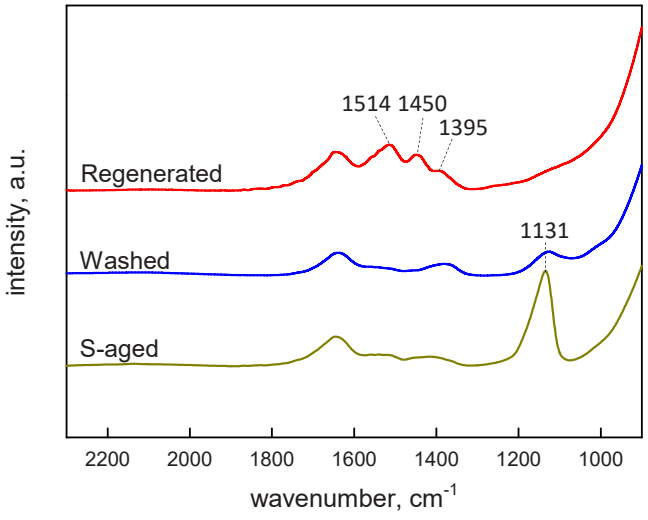

Fig. 3. FT-IR spectra recorded on S-aged, washed and regenerated Li-Ru DFM samples after stabilization in air.

the parent RuA catalyst [34], showing a main band at ca 1383 cm^{-1} due to bicarbonates formed on Al-hydroxylated sites. Eventually, the replenishment of the alkali content in the washed DFM via impregnation (and subsequent H_2-reduction) promoted the adsorption of CO_2 from the air at room temperature, causing the appearance of the two additional bands at 1514, 1448 cm^{-1} (assigned to bidentate carbonates and bicarbonates [37]), which are characteristic of the fresh Li-Ru DFM [34].

3.3. S-poisoning and regeneration of the catalytic functionality in Li-Ru DFM

Catalytic methanation tests run by co-feeding CO_2 and H_2 were used as a sensitive tool to investigate the S-poisoning effects and the regeneration of the catalytic Ru sites in the DFM. Results are presented in Fig. 4 in terms of the CO_2 conversion and selectivity to CH_4 as a function of the reaction temperature, and in Fig. 5 in terms of the specific reaction rate and CH_4 selectivity at 280 °C: note that CO was the only other C-bearing product apart from CH_4. Moreover, Table 1 reports the values of the temperature required to achieve 10% conversion (T_{10}) and the apparent activation energy for the CO_2 hydrogenation reaction.

The saturation of the basic Li sites on the surface of the S-aged DFM, which was caused by the formation of Li_2SO_4, lowered the intrinsic methanation activity of the Ru catalyst, thus shifting the relevant conversion plot in Fig. 4a towards higher temperatures [34]. In particular, Fig. 5 shows the reaction rate per unit volume of the S-aged DFM dropped by a factor close to 3 at 280 °C, whereas the selectivity to CH_4 was not affected. Moreover, the large accumulation of sulfates on the S-aged DFM made it prone to a self-poisoning effect: when the reaction temperature exceeded the threshold level of ca 290 °C, we observed a significant inhibition of the catalytic activity (Fig. 4a) and a simultaneous loss of CH_4 selectivity (Fig. 4b) during the temperature programmed methanation test. This is consistent with sulfate species over the S-aged DFM starting to react with H_2 on the top of the catalytic Ru nanoparticles to form inactive RuS_x species [32–34]. The extent of poisoning depended on time and temperature: after exposing the same

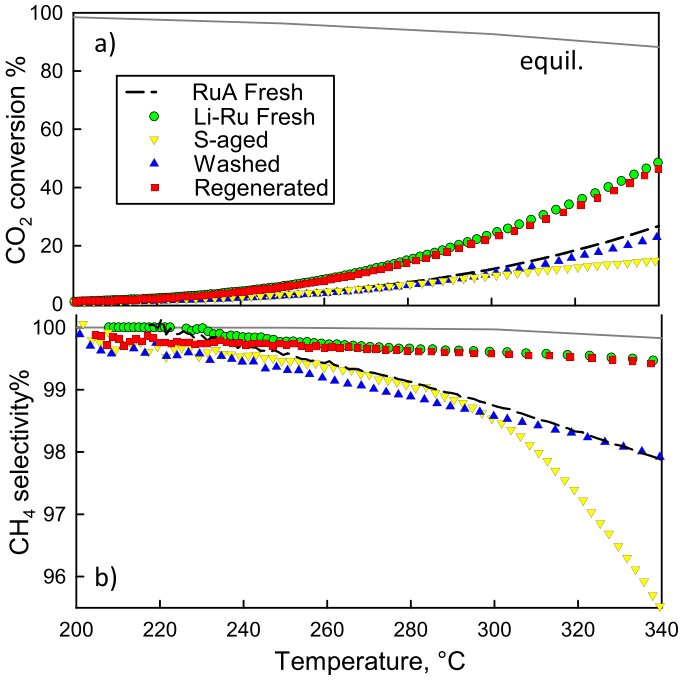

Fig. 4. CO_2 conversion (a) and selectivity to CH_4 (b) as a function of the reaction temperature during the catalytic methanation tests over the fresh, S-aged, washed and regenerated Li-Ru DFM samples as well as the reference RuA catalyst. Feed composition: $CO_2/H_2/N_2 = 1/4/5$, GHSV = 33000 h^{-1}. The solid lines correspond to the thermodynamic equilibrium curves.

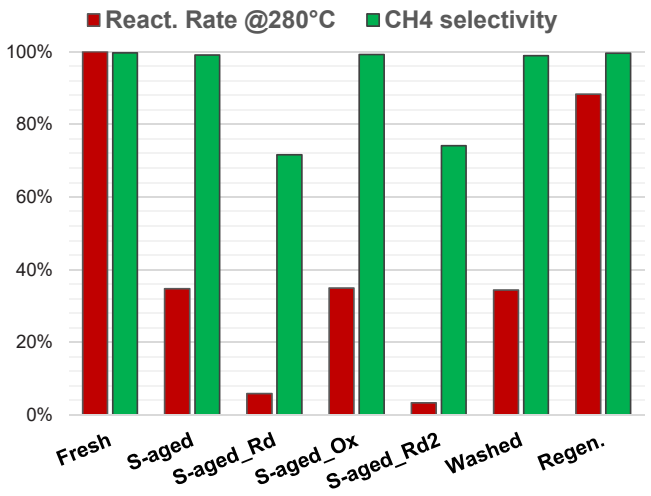

Fig. 5. CO_2 hydrogenation rate (per unit volume, normalized to the fresh sample) and CH_4 selectivity at 280 °C over the fresh, S-aged, washed and regenerated Li-Ru DFM. Repeated tests on the S-aged DFM were run after exposing the sample to reaction conditions at 400 °C (_Rd; _Rd2) or after oxidizing it in air at 300 °C (_Ox). Experimental conditions as in Fig. 4.

S-aged DFM for 30 min at 400 °C to reaction (i.e. reducing) conditions, its residual reaction rate (S-aged_Rd in Fig. 5) dropped down to less than 5% of the original value over the fresh DFM.

However, this self-poisoning effect could be fully reversed via an oxidative treatment under mild conditions. As shown in Fig. 5 (S-aged_Ox), the S-aged DFM recovered its catalytic activity (and selectivity) if it was pre-oxidized with air at 300 °C before the new methanation run. As expected, the self-poisoning effect manifested once again when the DFM was re-exposed to reaction conditions at temperatures above 290 °C (S-aged_Rd2 in Fig. 5). The mechanism behind the oxidative regeneration of S-poisoned Ru nanoparticles was previously described [32,33] and depends on the peculiar characteristic of the inactive RuS_x species, which can be directly decomposed into RuO_x and SO_2 without forming stable sulfates: this allows the full recovery of the catalytic activity once Ru is reduced back to its metal form (i.e. as soon as it is exposed to H_2 at T > 150 °C).

It can be concluded that the remarkable sulfur-tolerance displayed by the Li-Ru DFM during the integrated CO_2 capture and methanation cycles comes from two main reasons: i) the high intrinsic catalytic activity of this DFM allows to optimally operate the process at temperatures as low as 260 – 280 °C [34], where sulfur is stably stored as Li_2SO_4 and self-poisoning effects are not likely to occur; ii) the existence of a peculiar self-regeneration mechanism related to the redox properties of Ru, which can naturally remove any RuS_x species possibly formed on the heavily sulfated-DFM during the hydrogenation step by oxidizing and simultaneously decomposing them during the CO_2 capture in the presence of molecular oxygen [24].

Catalytic activity measurements performed on the washed DFM confirmed this picture: at low temperatures, the conversion and selectivity plots were roughly superimposed to the corresponding plots relevant to the S-aged sample as well as to the unpromoted RuA catalyst (Fig. 4). However, no self-poisoning effect was observed for T > 290 °C because (most of) the Li_2SO_4 had been already removed by washing and the resulting DFM sample behaved as the unpromoted RuA catalyst in the whole range of temperatures explored.

Ultimately, the replenishment of Li content in the regenerated DFM effectively restored the original catalytic methanation activity of the fresh DFM, as shown by the superimposed conversion and selectivity plots (Fig. 4) as well as corresponding T_{10} values. Furthermore, the apparent activation energy values for the fresh and regenerated DFMs were identical and equal to 81 KJ mol^{-1}. It can be argued that the presence of surface basic Li-sites close to Ru nanoparticles boosted their

catalytic activity more than the type of support (Li-aluminate vs. pure γ-Al_2O_3) they were dispersed on. This also induced a characteristic increase in the apparent activation energy (ca + 10–12 kJ mol^{-1}) with respect to either the unpromoted, sulfated or washed counterparts (Table 1). Eventually, it is worth noting that the moderate but irreversible sintering of Ru nanoparticles suggested by the XRD analysis of the aged DFM translated only into a minor adverse impact (ca −10%) on the specific reaction rate of the regenerated DFM at 280 °C (Regen, Fig. 5).

3.4. *Operando DRIFT characterization of ICCM over fresh and S-aged DFMs*

Fig. 6a shows two main bands at ca 1620 cm^{-1} and at 1357 cm^{-1} with shoulders at 1558 and 1410 cm^{-1} arising soon after the CO_2 reached the fresh (pre-reduced) DFM: their intensity increased rapidly during the first 2–3 min on stream and then saturated, confirming the fast kinetics of the CO_2 adsorption on the activated Li-Ru DFM at 300 °C [18,35]. The main bands can be assigned to bidentate carbonates chemisorbed on the Li doped alumina (at 1605 and 1355 cm^{-1}, respectively chelating and bridged; at 1545 cm^{-1}, asymmetric stretching on hydrotalcite type Li-Al compound) [35,38,39] but they also include additional contributions from more weakly bound (physisorbed) bicarbonates (at 1645 and 1430 cm^{-1}) [35,40]. The small yet clear spectral feature appearing in the range 1900–1810 cm^{-1}, with a maximum at 1840–1850 cm^{-1}, was due to CO adsorbed on low coordination Ru^0 sites in bridging configuration [25,35,41,42], which was most probably formed by the H-assisted dissociation of some CO_2 spilling over from the support onto the nearby reduced noble metal nanoparticles. After purging with Ar for 30 min (first spectrum in Fig. 6b at t = 0), the intensity of the two maxima of the carbonate bands, as well as the Δν in between them, decreased as a consequence of the removal of weakly bound bicarbonate species, still leaving a significant amount of adsorbed CO_2 available for the subsequent hydrogenation. Also, those carbonyls on Ru were preserved, in good agreement with previous results reported on Ru/Al_2O_3 [35,43]. During the subsequent reduction step with 2% H_2 at the same temperature, the amount of bidentate carbonates was progressively consumed to form methane (and no CO), as confirmed by the small signal appearing at ca 3015 cm^{-1} (not shown), whose intensity reached a maximum at 5 min and slowly decreased thereafter. Simultaneously, a new band appeared centred at ~1990 cm^{-1}, whose intensity followed the same temporal evolution of methane, reaching a maximum soon after the beginning of the hydrogenation phase. This spectral feature can be associated with novel carbonyl species in various bridged configurations on Ru [22], and it was also observed after H_2 adsorption on ruthenium with pre-adsorbed CO [42]. Interestingly, this new band didn't replace the original one at ca 1840 cm^{-1} related to carbonyls formed during CO_2 adsorption: both signals were maximum in the initial phase of the hydrogenation (red spectrum in Fig. 6b) and they slowly and simultaneously diminished along with time on stream. This suggests a role for both types of carbonyls and the possible migration of adsorbed CO species that are continuously replenished via the reverse spill-over of bidentate carbonates from the Li-Al support across the interface with the active metal nanoparticles, where they can finally react with the co-adsorbed -H atoms present under the H_2 flow. Analogue transient FT-IR results were recently reported in [22] for a Ru,"Na_2O"/Al_2O_3 DFM, confirming the role of adsorbed CO as an intermediate product in the methanation of

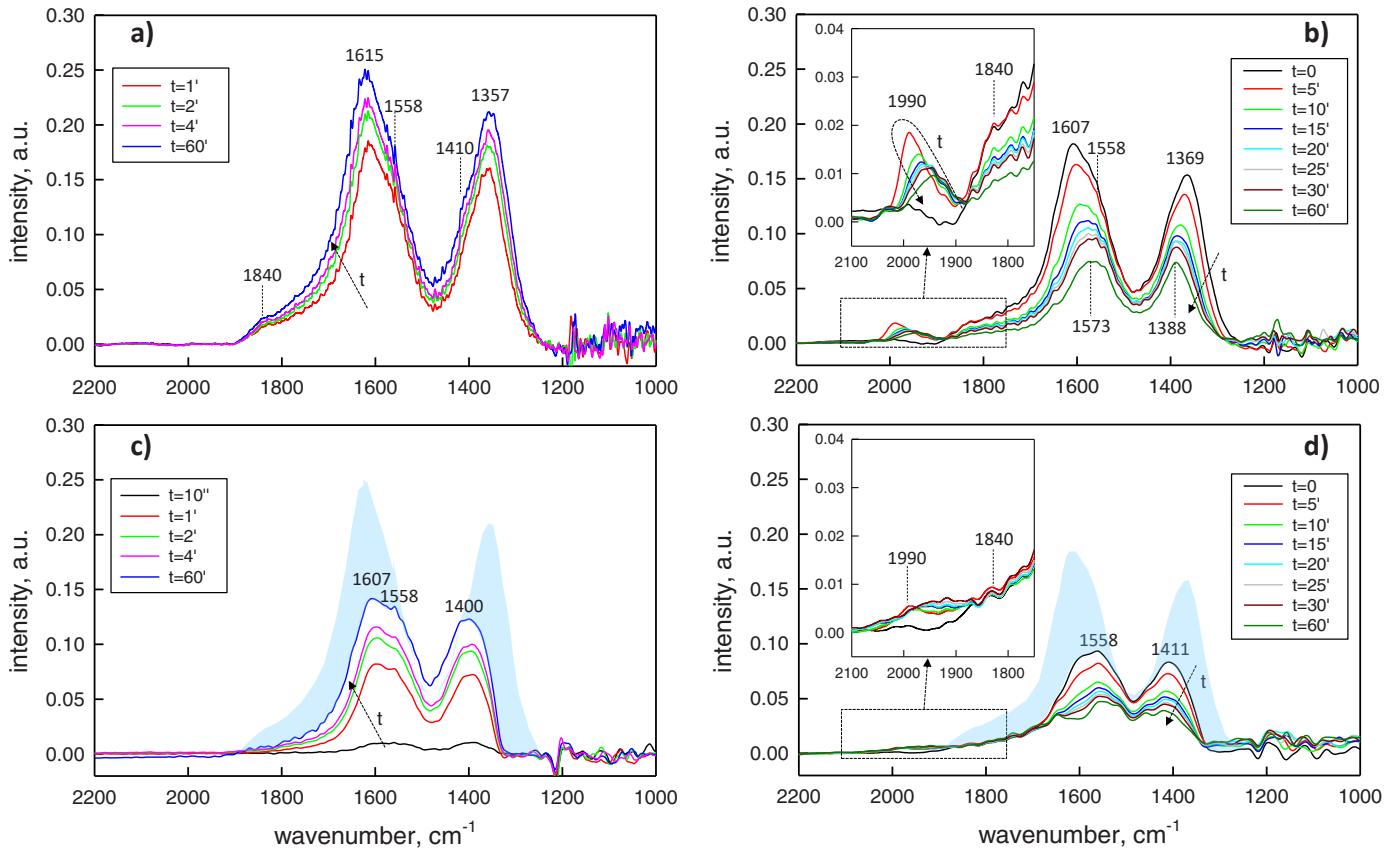

Fig. 6. In-situ transient DRIFT spectra during the CO_2 capture (a, c) and subsequent hydrogenation (b, d) at 300 °C on the fresh (a,b) and S-aged (c,d) Li-Ru DFM. Shaded areas in panels (c) and (d) highlight the difference between corresponding spectra at the end of the carbonation and after the intermediate purge just before the hydrogenation phase, respectively. DFM samples pretreated at 400 °C under 2% H_2 in N_2. Feed sequence: 15% CO_2 in N_2, 60 min; inert purge, 30 min; 2% H_2 in N_2, 60 min. Experimental details can be found in Section 2.2.

pre-captured CO_2 over alkali-promoted Ru DFMs [22,25,38].

Fig. 6c,d show the corresponding results of the transient DRIFT characterization during the CO_2 capture and subsequent hydrogenation at 300 °C on the S-aged Li-Ru DFM sample: the two shaded areas represent the difference between the spectra acquired over the fresh and S-aged DFM at the end of the CO_2 capture (panel c) and just before the hydrogenation phase (panel d). Carbonation of the S-aged DFM proceeded with the same qualitative dynamic observed in the case of the fresh sample, but the intensity of the bands due to bidentate carbonates was significantly reduced and their maxima were slightly shifted at 1607 and 1400 cm^{-1}. This is a direct consequence of the extensive formation of Li_2SO_4 species on the S-aged DFM that irreversibly blocked the basic Li-Al adsorption sites and, in turn, limited the CO_2 capture capacity of the sample. Moreover, the carbonyl species in the bridged configuration observed on the fresh DFM (at 1840–1850 cm^{-1}) were severely reduced and barely detectable on the S-aged sample. A similar effect was reported for a reaction-aged Ru,"Na_2O" DFM and ascribed to the strong loss of exposed Ru surface area due to sintering caused by the prolonged looping operation at 320 °C [22]. At variance, in the present case the sintering of Ru nanoparticles was shown to be rather limited (Table 1): therefore, the apparent loss of the active metal surface area can be assigned to a shielding effect due to the presence of Li_2SO_4 at the metal support interface and/or to the formation of RuS_x species following the reductive pretreatment of the S-aged DFM at 400 °C in H_2. It is worth recalling that the same reductive treatment at 400 °C caused a severe deactivation of the S-aged DFM sample during the catalytic methanation tests (Fig. 5) due to the self-poisoning mechanism involving the reaction of the sulfate species stored on the DFM.

As for the fresh sample, purging the S-aged DFM under Ar flow removed a further quantity of adsorbed CO_2 (Fig. 6d, black line at t = 0) corresponding to bicarbonates and some more weakly bound bidentate carbonates. During the hydrogenation step, the bands of the residual adsorbed carbonates, initially showing their maxima at 1586 and 1400 cm^{-1}, were progressively consumed. However, the intensity of the band at 1990 cm^{-1} relevant to bridged carbonyls on Ru, which appeared during the hydrogenation, was much lower (inset of Fig. 6d), once again confirming the limited availability of active surface Ru sites free from S on this DFM sample.

All the original features described for the fresh DFM were detected during the operando DRIFT characterization of the regenerated sample (not shown), including the small carbonyl band at 1840 cm^{-1}, which, on the contrary, was absent in the spectra relevant to the washed DFM, thus confirming the effectiveness of the regeneration treatment.

4. Conclusions

Li-Ru/Al_2O_3 Dual Function Materials can operate the Integrated CO_2 Capture and Methanation at low temperatures showing a remarkable tolerance to SO_2 impurities, which are trapped and stored as Li_2SO_4. Long-term accumulation of sulfates on the DFM affects its CO_2 capture capacity, but only to a minor extent its catalytic methanation activity. To address this issue, a simple ex-situ procedure was developed to regenerate the spent DFM aiming to minimize the consumption of a critical raw material like Ru within a circular economy approach. In particular, by washing the S-aged DFM in demineralized water at room temperature it was possible to remove the sulfur loading while preserving the original Ru content. Eventually, by replenishing the initial Li loading via a novel impregnation with nitrate precursor, the CO_2 capture capacity of the regenerated DFM was fully restored up to the original level, as it was the catalytic methanation activity per unit mass of Ru. Repeated tests of the ICCM process in a fixed bed at 260 °C under S-free feed conditions demonstrated the regeneration treatment was highly effective in restoring the initial performance of the fresh DFM.

Detailed ex-situ and operando characterization of the fresh, the S-aged, and the regenerated DFM samples highlighted that the selective S-poisoning of Ru nanoparticles is prevented due to the stability of the Li-sulfate species at the low operating temperature required by such highly active DFM. A self-poisoning effect can manifest over the heavily sulfated DFM only when the hydrogenation temperature exceeds 290 °C, which promotes the formation of inactive RuS_x species on the top of the Ru nanoparticles. However, Ru-sulfides can be easily decomposed as soon as the DFM is exposed to the typical oxidizing conditions encountered during the subsequent CO_2 capture phase, which naturally entails a periodic regeneration mechanism for the catalytic functionality.

Funding

This research was partially funded by the European Union – Next-Generation EU from the Italian Ministry of Environment and Energy Security POR H_2 AdP MMES/ENEA with involvement of CNR and RSE, PNRR - Mission 2, Component 2, Investment 3.5 "Ricerca e sviluppo sull'idrogeno", CUP: B93C22000630006.

CRediT authorship contribution statement

Stefano Cimino: Conceptualization, Investigation, Data curation, Writing – original draft, Writing – review & editing, Supervision, Funding acquisition. **Elisabetta Maria Cepollaro:** Investigation, Data curation. **Milena Pazzi:** Investigation. **Luciana Lisi**: Investigation, Conceptualization, Writing – original draft, Writing – review & editing.

Declaration of Competing Interest

The authors declare that they have no known competing financial interests or personal relationships that could have appeared to influence the work reported in this paper.

Data Availability

Data will be made available on request.

References

[1] J. Mertens, C. Breyer, K. Arning, A. Bardow, R. Belmans, A. Dibenedetto, S. Erkman, J. Gripekoven, G. Léonard, S. Nizou, D. Pant, A.S. Reis-Machado, P. Styring, J. Vente, M. Webber, C.J. Sapart, Carbon capture and utilization: more than hiding CO_2 for some time, Joule (2023) 1–8, https://doi.org/10.1016/j.joule.2023.01.005.

[2] S. Saeidi, S. Najari, V. Hessel, K. Wilson, F.J. Keil, P. Concepción, S.L. Suib, A. E. Rodrigues, Recent advances in CO_2 hydrogenation to value-added products — Current challenges and future directions, Prog. Energy Combust. Sci. 85 (2021), 100905, https://doi.org/10.1016/j.pecs.2021.100905.

[3] B. Shao, Y. Zhang, Z. Sun, J. Li, Z. Gao, Z. Xie, J. Hu, H. Liu, CO_2 capture and in-situ conversion: recent progresses and perspectives, Green Chem. Eng. 3 (2022) 189–198, https://doi.org/10.1016/j.gce.2021.11.009.

[4] S. Sun, H. Sun, P.T. Williams, C. Wu, Recent advances in integrated CO_2 capture and utilization: a review, Sustain. Energy Fuels 5 (2021) 4546–4559, https://doi.org/10.1039/d1se00797a.

[5] I.S. Omodolor, H.O. Otor, J.A. Andonegui, B.J. Allen, A.C. Alba-Rubio, Dual-function materials for CO_2 capture and conversion: a review, Ind. Eng. Chem. Res. 59 (2020) 17612–17631, https://doi.org/10.1021/acs.iecr.0c02218.

[6] Z. Sun, B. Shao, Y. Zhang, Z. Gao, M. Wang, H. Liu, J. Hu, Integrated CO_2 capture and methanation from the intermediate-temperature flue gas on dual functional hybrids of AMS/CaMgO||Ni Co, Sep. Purif. Technol. 307 (2023), 122680.

[7] S. Sun, Z. Lv, Y. Qiao, C. Qin, S. Xu, C. Wu, Integrated CO_2 capture and utilization with CaO-alone for high purity syngas production, Carbon Capture Sci. Technol. 1 (2021), 100001, https://doi.org/10.1016/J.CCST.2021.100001.

[8] L.-P. Merkouri, T.R. Reina, M.S. Duyar, Closing the carbon cycle with dual function materials, Energy Fuels (2021), https://doi.org/10.1021/acs.energyfuels.1c02729.

[9] P. Melo Bravo, D.P. Debecker, Combining CO_2 capture and catalytic conversion to methane, Waste Dispos. Sustain. Energy 1 (2019) 53–65, https://doi.org/10.1007/s42768-019-00004-0.

[10] F. Kosaka, Y. Liu, S.-Y. Chen, T. Mochizuki, H. Takagi, A. Urakawa, K. Kuramoto, Enhanced activity of integrated CO_2 capture and reduction to CH4 under pressurized conditions toward atmospheric CO_2 utilization, ACS Sustain. Chem. Eng. 9 (2021) 3452–3463, https://doi.org/10.1021/acssuschemeng.0c07162.

[11] J. Chen, Y. Xu, P. Liao, H. Wang, H. Zhou, Recent progress in integrated CO_2 capture and conversion process using dual function materials: a state-of-the-art

review, Carbon Capture Sci. Technol. 4 (2022), 100052, https://doi.org/10.1016/j.ccst.2022.100052.
[12] L. Merkouri, A.I. Paksoy, T. Ramirez Reina, M.S. Duyar, The need for flexible chemical synthesis and how dual-function materials can pave the way, ACS Catal. (2023) 7230–7242, https://doi.org/10.1021/acscatal.3c00880.
[13] M.S. Duyar, S. Wang, M.A. Arellano-Treviño, R.J. Farrauto, CO_2 utilization with a novel dual function material (DFM) for capture and catalytic conversion to synthetic natural gas: an update, J. CO_2 Util. 15 (2016) 65–71, https://doi.org/10.1016/j.jcou.2016.05.003.
[14] F. Kosaka, T. Sasayama, Y. Liu, S. Chen, T. Mochizuki, K. Matsuoka, A. Urakawa, K. Kuramoto, Direct and continuous conversion of flue gas CO_2 into green fuels using dual function materials in a circulating fluidized bed system, Chem. Eng. J. 450 (2022), 138055, https://doi.org/10.1016/j.cej.2022.138055.
[15] M.S. Duyar, M.A.A. Treviño, R.J. Farrauto, Dual function materials for CO_2 capture and conversion using renewable H2, Appl. Catal. B Environ. 168–169 (2015) 370–376, https://doi.org/10.1016/j.apcatb.2014.12.025.
[16] M. Abdallah, R. Farrauto, A perspective on bridging academic research and advanced testing on a path towards pilot plant implementation: a case study of integrating CO_2 capture and catalytic conversion with dual function materials, Catal. Today (2022), https://doi.org/10.1016/j.cattod.2022.10.005.
[17] A. Bermejo-López, B. Pereda-Ayo, J.A. González-Marcos, J.R. González-Velasco, Mechanism of the CO_2 storage and in situ hydrogenation to CH_4. Temperature and adsorbent loading effects over Ru-CaO/ Al_2O_3 and Ru-Na_2CO_3/ Al_2O_3 catalysts, Appl. Catal. B Environ. 256 (2019), 117845, https://doi.org/10.1016/J.APCATB.2019.117845.
[18] S. Cimino, F. Boccia, L. Lisi, Effect of alkali promoters (Li, Na, K) on the performance of Ru/Al_2O_3 catalysts for CO_2 capture and hydrogenation to methane, J. CO_2 Util. 37 (2020) 195–203, https://doi.org/10.1016/j.jcou.2019.12.010.
[19] A. Porta, R. Matarrese, C.G. Visconti, L. Castoldi, L. Lietti, Storage material effects on the performance of Ru-based CO_2 capture and methanation dual functioning materials, Ind. Eng. Chem. Res. 60 (2021) 6706–6718, https://doi.org/10.1021/acs.iecr.0c05898.
[20] M.A. Arellano-Treviño, Z. He, M.C. Libby, R.J. Farrauto, Catalysts and adsorbents for CO_2 capture and conversion with dual function materials: limitations of Ni-containing DFMs for flue gas applications, J. CO_2 Util. 31 (2019) 143–151, https://doi.org/10.1016/j.jcou.2019.03.009.
[21] A.I. Tsiotsias, N.D. Charisiou, I.V. Yentekakis, M.A. Goula, The role of alkali and alkaline earth metals in the CO_2 methanation reaction and the combined capture and methanation of CO_2, Catalysts 10 (2020) 1–36, https://doi.org/10.3390/catal10070812.
[22] C. Jeong-Potter, A. Porta, R. Matarrese, C.G. Visconti, L. Lietti, R. Farrauto, Aging study of low Ru loading dual function materials (DFM) for combined power plant effluent CO_2 capture and methanation, Appl. Catal. B Environ. 310 (2022), 121294, https://doi.org/10.1016/j.apcatb.2022.121294.
[23] A. Bermejo-López, B. Pereda-Ayo, J.A. Onrubia-Calvo, J.A. González-Marcos, J. R. González-Velasco, Aging studies on dual function materials Ru/Ni-Na/Ca-Al2O3 for CO_2 adsorption and hydrogenation to CH4, J. Environ. Chem. Eng. 10 (2022), 107951, https://doi.org/10.1016/j.jece.2022.107951.
[24] S. Cimino, E.M. Cepollaro, L. Lisi, Sulfur tolerance and self-regeneration mechanism of Na-Ru/Al2O3 dual function material during the cyclic CO_2 capture and catalytic methanation, Appl. Catal. B Environ. 317 (2022), 121705, https://doi.org/10.1016/j.apcatb.2022.121705.
[25] C. Jeong-Potter, M. Abdallah, C. Sanderson, M. Goldman, R. Gupta, R. Farrauto, Dual function materials (Ru+Na2O/Al2O3) for direct air capture of CO_2 and in situ catalytic methanation: the impact of realistic ambient conditions, Appl. Catal. B Environ. 307 (2022), 120990.
[26] A.K. Das, J. De Wilde, G.J. Heynderickx, G.B. Marin, S.B. Iversen, K. Felsvang, Simultaneous adsorption of SO2 - NOx from flue gases in a riser configuration, AIChE J. 47 (2001) 2831–2844, https://doi.org/10.1002/aic.690471220.
[27] A. Porta, C.G. Visconti, L. Castoldi, R. Matarrese, C. Jeong-Potter, R. Farrauto, L. Lietti, Ru-Ba synergistic effect in dual functioning materials for cyclic CO_2 capture and methanation, Appl. Catal. B Environ. 283 (2021), 119654, https://doi.org/10.1016/j.apcatb.2020.119654.
[28] González-Marcos, J.R. González-Velasco, How the presence of O2 and NOx influences the alternate cycles of CO_2 adsorption and hydrogenation to CH4 on Ru-Na-Ca/Al2O3 dual function material, J. CO_2 Util. 67 (2023), 102343, https://doi.org/10.1016/J.JCOU.2022.102343.
[29] M. Argyle, C. Bartholomew, Heterogeneous catalyst deactivation and regeneration: a review, Catalysts 5 (2015) 145–269, https://doi.org/10.3390/catal5010145.
[30] S. Cimino, R. Torbati, L. Lisi, G. Russo, Sulphur inhibition on the catalytic partial oxidation of methane over Rh-based monolith catalysts, Appl. Catal. A Gen. 360 (2009) 43–49, https://doi.org/10.1016/j.apcata.2009.02.045.
[31] B. Legras, V.V. Ordomsky, C. Dujardin, M. Virginie, A.Y. Khodakov, Impact and detailed action of sulfur on methane synthesis on Ni/γ-Al_2O_3 catalyst, ACS Catal. 4 (2014) 2785–2791, https://doi.org/10.1021/cs500436f.
[32] D. Kuzmenko, M. Nachtegaal, C. Copéret, T.J. Schildhauer, Molecular-level understanding of support effects on the regenerability of Ru-based catalysts in the sulfur-poisoned methanation reaction, J. Catal. 375 (2019) 74–80, https://doi.org/10.1016/j.jcat.2019.04.019.
[33] D. Kuzmenko, A.H. Clark, T. Schildhauer, J. Szlachetko, M. Nachtegaal, Operando sulfur speciation during sulfur poisoning-regeneration of Ru/SiO_2 and Ru/Al_2O_3 using non-resonant sulfur Kα 1,2 emission, RSC Adv. 10 (2020) 15853–15859, https://doi.org/10.1039/D0RA03068F.
[34] S. Cimino, E.M. Cepollaro, L. Lisi, Ageing study of Li-Ru/Al2O3 dual function material during the integrated CO_2 capture and methanation with SO_2-containing flue gas, Carbon Capture Sci. Technol. 6 (2023), 100096.
[35] S. Cimino, R. Russo, L. Lisi, Insights into the cyclic CO_2 capture and catalytic methanation over highly performing Li-Ru/Al_2O_3 dual function materials, Chem. Eng. J. 428 (2022), 131275, https://doi.org/10.1016/j.cej.2021.131275.
[36] S.U. Rege, R.T. Yang, A novel FTIR method for studying mixed gas adsorption at low concentrations: H_2O and CO_2 on NaX zeolite and γ-alumina, Chem. Eng. Sci. 56 (2001) 3781–3796, https://doi.org/10.1016/S0009-2509(01)00095-1.
[37] T. Montanari, L. Castoldi, L. Lietti, G. Busca, Basic catalysis and catalysis assisted by basicity: FT-IR and TPD characterization of potassium-doped alumina, Appl. Catal. A Gen. 400 (2001) 61–69, https://doi.org/10.1016/j.apcata.2011.04.016.
[38] L. Proaño, E. Tello, M.A. Arellano-Trevino, S. Wang, R.J. Farrauto, M. Cobo, In-situ DRIFTS study of two-step CO_2 capture and catalytic methanation over Ru,"Na_2O"/Al_2O_3 Dual Functional Material, Appl. Surf. Sci. 479 (2019) 25–30, https://doi.org/10.1016/j.apsusc.2019.01.281.
[39] K. Coenen, F. Gallucci, B. Mezari, E. Hensen, M. van Sint Annaland, An in-situ IR study on the adsorption of CO_2 and H_2O on hydrotalcites, J. CO_2 Util. 24 (2018) 228–239, https://doi.org/10.1016/j.jcou.2018.01.008.
[40] L. Falbo, C.G. Visconti, L. Lietti, J. Szanyi, The effect of CO on CO_2 methanation over Ru/Al_2O_3 catalysts: a combined steady-state reactivity and transient DRIFT spectroscopy study, Appl. Catal. B: Environ. 256 (2019), 117791.
[41] B. Miao, S.S.K. Ma, X. Wang, H. Su, S.H. Chan, Catalysis mechanisms of CO_2 and CO methanation, Catal. Sci. Technol. 6 (2016) 4048–4058, https://doi.org/10.1039/C6CY00478D.
[42] H.I. Hadjiivanov, G.N. Vaysilov, Characterization of oxide surfaces and zeolites by carbon monoxide as an IR probe molecule, Adv. Catal. 47 (2002) 307–511.
[43] X. Wang, Y. Hong, H. Shi, J. Szanyi, Kinetic modeling and transient DRIFTS-MS studies of CO_2 methanation over Ru/Al2O3 catalysts, J. Catal. 343 (2016) 185–195, https://doi.org/10.1016/j.jcat.2016.02.001.